The Bioscan AN INTERNATIONAL QUARTERLY JOURNAL OF LIFE SCIENCES 19(1): 62-72, 2025 www.thebioscan.com

GREEN SYNTHESIS OF GOLD NANOPARTICLES USING BROWN SEAWEED OF SARGASSUM TENERRIMUM AND EVALUATION OF THEIR ANTICANCERAL AND CATALYTIC ACTIVITY

V. Parthiban[1*], K. Kalarani[2]

1. Assistant Professor of chemistry, Pope's College (Autonomous), Sawyerpuram, Affiliated to Manonmaniam Sundaranar University, Tirunelveli

2. Assistant Professor of chemistry, Kamaraj College (Autonomous) Thoothukudi, Affiliated to Manonmaniam Sundaranar university, Tirunelveli

corresponding author - parthiban370@gmail.com

DOI: 10.63001/tbs.2024.v19.i01.pp62-72

KEYWORDS
Anticancer, Catalytic activity, Gold nanoparticle, Seaweed, Synthesis.
Received on:

18-07-2024

Accepted on:

23-08-2024

Published on

27-09-2024

ABSTRACT

In biomedical science, the utilization of gold nanoparticles becomes enriched. In recent times, it has been stated that natural products act as agents that reduce and stabilize the raw mass of metal nanoparticles. Nanoparticles are classified using the ultraviolet-visible spectrum, X-ray diffraction (XRD), transmission electron microscopy (TEM) and scanning & fundamental (SEM & EDX),. The nanoparticles are round and crystalline around < 20 nm in size. Cancerous SK MEL-28 cells have shown evidence of anticancer action. The integrity of SK MEL-28 cells was determined by trypan's green test. The nature of drug release responds to *Sargassum tenerrimum* and inhibits the growth of cancer cells by AuNPs.Nanoparticles compacted by such environmentally friendly methods can be utilized to combine multiple metal nanoparticles and active catalysts for a wide range of biomedical resources, large commerce production & various biological reactions.

INTRODUCTION

Nanoparticles are getting more attention in numerous research fields like material science chemistry, biology, physics, and engineering owing to their unique properties such as catalytic, magnetic, optical, and electronic as well as the unique feature of their shape and size [1, 2]. Numerous chemical and physical systems are affected by the harmful chemicals and unavailability of clinical equipment because of the toxic capping agents [3, 4]. Therefore, it leads to the use of different new techniques and components for generating the nanoparticles concerning the nano chemistry principles. The primary advantage of this technique is, it incorporates the nanoparticles for a large community with a lower effect on the ecosystem. Numerous academic and commercial investigators have focused on biological processes like plants, algae, fungi, and bacteria to make nanoparticles since their structure and potential applications are crucial [5–9]. Extract compounds function as an agent for lessening and stabilizing the nanoparticles and also provide more biocompatibility nanoparticles into biodegraded nanoparticles [10]. The primary source for several natural products is the ocean whereas seaweeds are part of the plant [11]. Moreover, Sponges are known to be an origin for the organisms such as vitamins, lipids, carotenoids, carbohydrates, metabolites, and proteins [12 - 14]. Furthermore, Other algae are also used including Kappaphycus alvarezii [17], Sargassum myriosystem [19], Acanthophora spicifera [15], Stoicospermum marginatum [20], Chlorella pyrenoidusa [16] and Sargassum weight [18]. Biosynthesized nanoparticles are validated for their pathogenesis to bacteria and various biological functions. At present, the impact of gold nanoparticles, cytotoxic (AuNPs) is ambiguous as well The effects of nanoparticles on cell distribution & function are unclear [21]. Therefore, the presented model defines the crude and effective approach to synthesizing a nanoparticle gold nanoparticle from the brown seaweed *Sargassum tenerimum* aqueous extract (*Sargassum tenerimum* immobilized AuNPs). The ability of AuNPs to cause cancer in vitro derived from stable Sargassum *tenerimum* was evaluated using SK MEL-28 cancer cell lines. Therefore, algae stand out as a future component of a crude set of nanoparticles. Moreover, At ambient temperature, the gold nanoparticles (AuNPs) performed as an effective catalyst. This structure has inspired several investigators to understand the performance of gold nanoparticles. In the construction field, Aromatic nitro compounds are mostly utilized chemical elements and also it is a very hazardous element to the environment. Even though, less amount of aromatic nitro solutions is utilized in hair dyes, polymers, components & pharmaceuticals used in rubber [22]. For the quenching progression, AuNPs become the effective catalysts. The impacts of toxic and product formation on reaction

media are unpopular, although chemically integrated AuNPs are considered ineffective catalysts and also give huge catalytic activity. Therefore, develop the active catalysts by chemical reduction. The primary reason for the pollution is dye from several fields such as paint, textile, and paper [23, 24]. The teeth of the chanterelles family namely rhodamine B and sulforothamine, are immensely dangerous and do not rust due to their harsh environmental effects. These dyes must be treated before they can be released into the atmosphere. Whereas, several chemical, physical and therapeutic agents are utilized to reduce the dye pollutants. However, these agents are not effective because it does not eject the pollutants, and also the operational cost is very high [25]. Therefore, in this work, by utilizing the aqueous extract of brown algae sargassum tenebrism the AuNPs are synthesized. The presented nanoparticles are considerably simple, effective, and inexpensive. Although there are many studies related to the biology of AuNPs derived via naturally extracted sources, app-based data are one or two, hence the test results on bioactive AuNPs worked as catalytic useful in nitric chemicals & dyes for discoloration. UV-based visible spectroscopy, scanning, elemental related microscopy (SEM & EDX), and X-ray diffraction (XRD), high-res transfer electron microscopy (HRTEM), & FTI (Fourier transform infrared) are useful in AuNP study.

1. METHODS

2.1Chemicals, Cell line, and materials

From the SRL chemical, India chloroauric acid was procured. From the Sigma Aldrich, p-nitroaniline, sulforhodamine 101, rhodamine, and 4-Nitrophenol were obtained. Moreover, in this study taken the maximum analytical grade contained reagents and chemicals. The National Center for Cell Science, India, Pune, given that SK MEL-28 (Malignant Melanoma) cell line. Brown algae *S. tenerrimum* species were gathered from the intertidal regions of the Tuticorin Coast of the Gulf of Mannar (latitude 8°47' North; longitude 78°8'E), Tamil Nadu, India, and brought to the laboratory. Plastic bag with seawater. Sublimation water was used to properly clean the algae material and remove any debris. The samples were dried in the shade, powdered, and preserved at 4º Celsius for further usage.

2.2 Preparation of extracts

To make the aqueous extract, 2 g of dried kelp was dissolved in 100 ml of distilled water. The extract was heated to 60 °C by a magnetic stirrer rotating at 180 rpm for 20 minutes before being filtered using Whatman No. 1 filter paper. Additionally, the filtered extracts underwent a 10-minute, 10,000 rpm centrifugation. Here, the supernatant was utilized as an agent for reduction as well as a stabilizer to prepare gold nanoparticles. When it was not utilized, the extract was cooled and preserved at 4 Celsius.

2.3 Synthesis in gold nanoparticles

In the 250 milliliter Erlenmeyer flask, the 50 ml-1mM aqueous $AuCl_4$ solution was mixed with the 5 ml algae aqueous extract. At room temperature, the Erlenmeyer flask was placed on a magnetic stirrer and the solution is transformed into a ruby red color that denotes the generation of gold nanoparticles. observing the decrease of the Au3+ ions for a certain interval in a given solution was done by UV–vis spectrophotometer. Once, it attains saturation, then for 15 minutes the gold nanoparticle 10000 rpm centrifuged the solution., & attained pellet was resuspended in distilled water for eliminating the unreacted biomass. The progression of centrifugation and the redistribution was performed two times to segregate the nanoparticles inefficiently way. The attained nanoparticles were lyophilized through the MiniLioDel lyophilizer.

1.4 Gold nanoparticles' characteristics

The addition of reduced green gold ions by culture supernatants of *S. tenerrimum* sp. A double beam UV-vis spectrophotometer (Perkin Elmer, Singapore) was used to conduct preliminary analysis for the different wavelengths.Furthermore, the synthesized gold nanoparticles were attained by repeating the centrifugation process for 15 minutes at 8000 rpm and dehydrated at ambient temperature. By utilizing the XRD, the nanoparticle's crystalline structure was analyzed (Bruker, Germany, model: D8Advance) and the morphological features like shape, distribution, and size were examined with SAED through the transmission electron microscope (Hitachi, model: S-3400N).

Furthermore, the average of the sound & the particle size arrangement of the nanoparticles (Joel JSM-6480 LV) were identified by the SEM machine. By utilizing the EDX, the existence of elemental gold was identified. The functionalized biomolecules attached to the gold nanoparticles it was categorized through the FT-IR (Bruker Optic GmbH model number - Tensor 27). Moreover, the nanoparticle sample was coupled with the KBr pellets and the wavelength was computed from 4000 to 400 cm−1.

1.5 The SK MEL-28 cell line is resistant to gold nanoparticles' anticancer effects.

The MTT assay is utilized for monitoring the activity of the cellular metabolic to denote the cytotoxicity, cell viability, and proliferation. A colorimetric test's fundamental process is the conversion of metabolically active cells into purple-hued formazan crystals from the yellow-hued tetrazolium salt (3-(4,5-dimethylthiazol-2-yl)-2,5-diphenyltetrazolium bromide, or MTT). MTT is additionally reduced to formazan by using NADPH-dependent oxidoreductase enzymes in living cells. The purple colour of the resulting solution is quantified using an ELISA plate reader at 570 nm, but insoluble formazan crystals are dissolved in a soluble solution (100 percent DMSO) [26].

2.6 Catalytic effect evaluation on synthesized gold nanoparticles

By using a UV spectrophotometer [27] catalytic bleaching process has been brought up with a three-milliliter quartz cuvette which has a one-centimeter length & is monitored according to Gangula et al. The icing mixture of $NaBH_4$ which consists of one milliliter of 0.03 m has been incorporated with an aquatic stock mixture of p-nitrophenol which has 0.03 milliliter of 0mM that collaborated with 1.4 milliliters of water. when the time, mixture of dispersed mixture which is 0.3 milliliter of the greened nanoparticles was added then the material was thoroughly blended. To monitor the previous progress's reaction, a 200-500 nanometer time-related absorption spectral was documented. However, Sulforhodamine 101 hydrate (SRH) & rhodamine B were considered to be the distinct organic solutions and Siddharth et al narrated that, nanoparticles could be utilized for catalytic purposes which had the above-mentioned dye compounds [28]. The significant nanoparticles of various volumes such as fifty, twenty-five &101 were represented as a catalytic component also the icing solution of $NaBH_4$ was collaborated with aquatic stocking compounds such as SRh & RhB. The process was further taken to the 450–700 nanometer range with UV spectral meter also at the greater room degrees, the mixture solution was ruffled.

3. RESULTS AND DISCUSSION

3.1 Visual inspection:

When algae extract was exposed to a gold ion solution, the color changed from brown shade to red-shaded ruby, which indicates a reduction of golden ions in gold nanoparticles. Also, the colour of that algae extracts changed from shaded brown to red-shaded ruby, when it collaborated with the golden ion complex solution, showing that gold ions were being reduced to gold nanoparticles. Colour change was detected; gold nanoparticles were found to have a diversity of colours as a result of their size and form [29]. The reaction time and phytochemical contents of the algae extract are the most important factors. The ruby red colour was created after 30 minutes of incubation, and the reduction process took 5 hours to complete. This might be related to the quick reduction of gold ion sands, which has been linked to the presence of significant reducing components in S. tenerrimum [30].

3.2 UV- Visible spectroscopy:

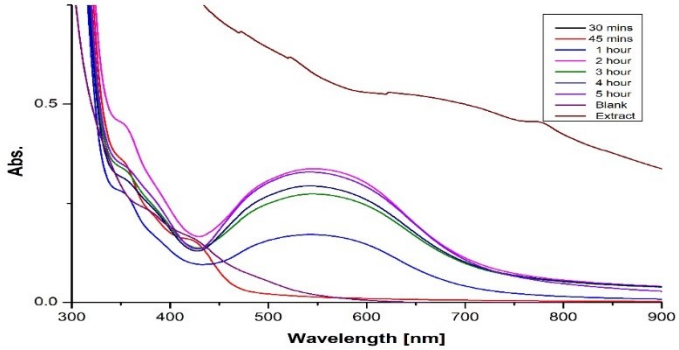

Figure 1: Green synthetic AuNPs from S. *tenerrimum* extract have UV-visible absorption spectra.

The most successful method is UV-Vis spectroscopy, to recognize the origination and solidity of AuNPs in an aqueous solution. Here, the reaction is performed at ambient temperature in a spectrophotometer with a resolution of 1 nm. The colloidal solution is examined through UV–a vis spectrophotometer. It is known that the maximum absorption of AuNPs ranges from 400 to 700 nm. The synthesis of AuNPs is examined at various time limits such as 30 min, 45 min, 60 min, 2 h, 3 h, 4 h 5 h. The AuNPs synthesized through seaweed extracts of *S. tenerrimum* were placed at 562 nm, (Figure 1) Initially, after 30 min, the AuNPs were slowly absorbed and the absorbance gradually increased over 5 h. Gopinath *et al* in 2013 reported that there was no such absorption that would be there for five hours which tells about the synthesis of au NP's completion[31]. The progression at different time limits exhibited absorption peaks at 562 nm matching the AuNPs surface plasmon resonance's wavelength [32]. Previous reviews have revealed that spherical gold nanoparticles present SPR bands within the UV-visible absorption spectra at approximately 525–555 nm because of the more-extraordinary nature and smaller dimension of the gold nanoparticles. The UV–Vis spectra of AuNPs from *T. arjuna cortex* extracts displayed a peak in absorption at 523 nm. *T. Arjuna cortex* which was derived by AuNP and the recent publication in 2018 Suganti *et al* represented the UV-visible immersion at a 536-nanometer rate [33]. Due to their tiny size and the presence of gold nanoparticles made by green synthesis, the SPR signal is becoming more pronounced [34] The UV-observed absorption spectrum confirms the small size & polydisperse nature of the green synthesized gold nanoparticles.

3.3 Fourier Transformed Infrared Spectroscopy:

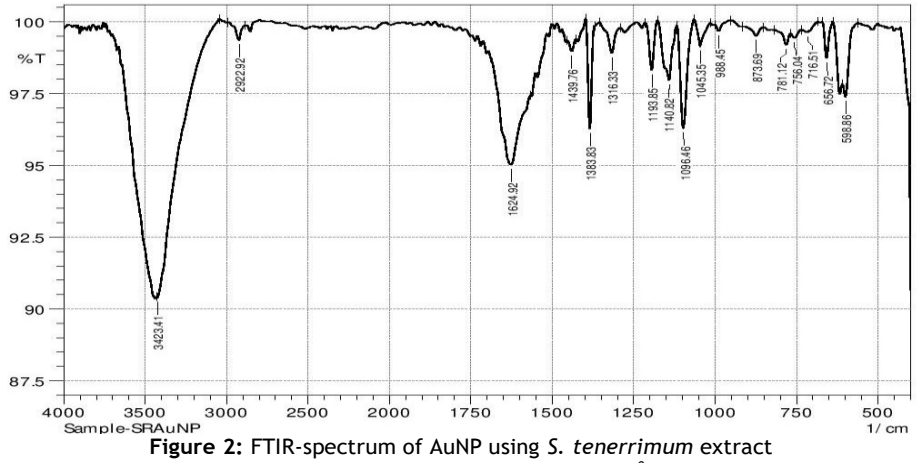

Figure 2: FTIR-spectrum of AuNP using *S. tenerrimum* extract

The FT-IR spectra extracts of *S. tenerrimum* exhibit peaks at 3423.41 cm−1 (NH stretch of primary amine), 2922.92 cm−1 (NH stretch of amine salt), 1624.92 cm−1 (C=O stretch of amide), 1439.76 cm− 1-1333.83 cm−1 (CH turn of alkane methyl group), 1316.33 cm−1 (OH turn of phenol), 1193.85 cm−1–1045.35 cm−1 (CO stretch of ester/lactone), 988.45 cm−1 (C) = C turn of mono substituted alkene), 781.12 cm–1 (C = C turn of vinylidene alkene), 756.04 cm–1 (C turn of 1,2,4 tri substituted), 716.51 cm–1 (C turn of 1,2) and 656.72 cm−1 - 598.86 cm−1 (C–Cl stretch of the halo compound). These absorption peaks occurred because of the existence of various functional groups like amides, esters, amine salts, alkanes. halogens, etc. The FT-IR results of the green synthesized gold nanoparticles utilizing the *S. tenerrimum* extract are shown in Fig. 2. The amine, amide, and hydroxyl groups of S. deviate in their signals in different ways. Establishment and immobilization of gold nanoparticles. In addition, three peaks occurred at 2922.92 cm−1, 1383.83 cm−1, and 1045.35 cm−1, equivalent to aldehyde, nitro, and ketone groups in the golden nanoparticles. However, peaks that are in the golden nanoparticles, symbolize that the amide is transformed to nitro also the alcohol groups to aldehyde/ketones to reduce $Au3^+$ ions to Au^0 green synthesized golden nanoparticles. Alkaloids, steroids, phenolic compounds, and amino acids—which are more typical of S. tenerrimum extracts—were found in higher concentrations in the peaks [35, 36]. The FT-IR outcomes recommend that alkaloids, steroids, phenolic compounds & amino acids presented in *S. tenerrimum* extracts were included in golden ions reduction. Also, these were adsorbed (or complexed) on the green synthesized gold nanoparticle's surface.

3.4 X-Ray Diffraction analysis:

XRD analysis was used to examine the degree of crystallinity and the size of gold nanoparticles produced using green synthesis and S. tenerrimum. A typical XRD design of green synthesized gold nanoparticles synthesized through the *S. As may be shown in Fig.3, tenerrimum extract was discovered to have an fcc structure.* The Bragg reflections at 2θ = 38.36°, 44.22°, 64.77° & 78.03º can be indexed to an orientation such as (111), (200), (220) & (311), which indicate the presence of the golden nanoparticles in fcc lattice plane (JCPDS-file number: 04-0784). Fig. 3 depicts the fcc structure that was discovered in *tenerrimum* extract. The mean crystalline diameter of gold nanoparticles green synthesized using *S.*

tenerrimum extract is 23 to 36 nm, as shown in Table 1 measured from the Debye–Scherer formula. The XRD results are comparable to an earlier study for gold nanoparticles [37] with *Dendropanax morbifera* leaf extract.

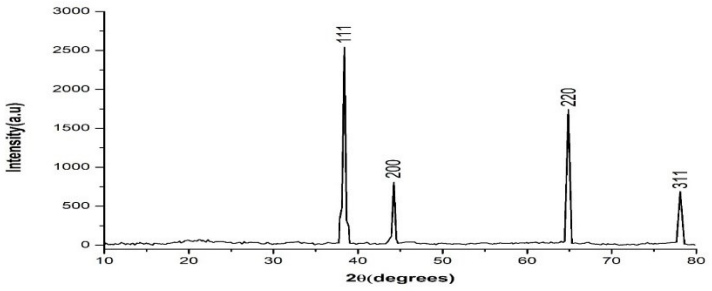

Figure 3: XRD patterns of AuNPs using *S. tenerrimum* extract

Table 1: XRD parameters of AuNPs using *S. tenerrimum* extract

Peak position 2θ (°)	FWHM B_{size} (°)	Crystalize size (nm)	Crystalize size Average (nm)
38.35758	0.38207	22.99	30.57
44.22328	0.27704	32.33	
64.76878	0.31949	30.75	
78.03252	0.295	36.20	

3.5 Scanning Electron Microscopy:

The size, surface morphology, and topography of the green-produced gold nanoparticles are all determined by SEM examination. *tenerrimum* extract. SEM images of green synthesized gold nanoparticles through *S. tenerrimum* extract, as shown in Figure 4. *S. tenerrimum* extract was spherical monodisperse. The usual dimension of the gold nanoparticles is between 20-34 nm. Due to the spectral shift, some agglomerated particles were also observed. Due to the stability of the nanoparticles with these protective chemicals, SEM pictures demonstrate that the tiniest gold nanoparticles have never been present in direct contact also inside the masses[38].

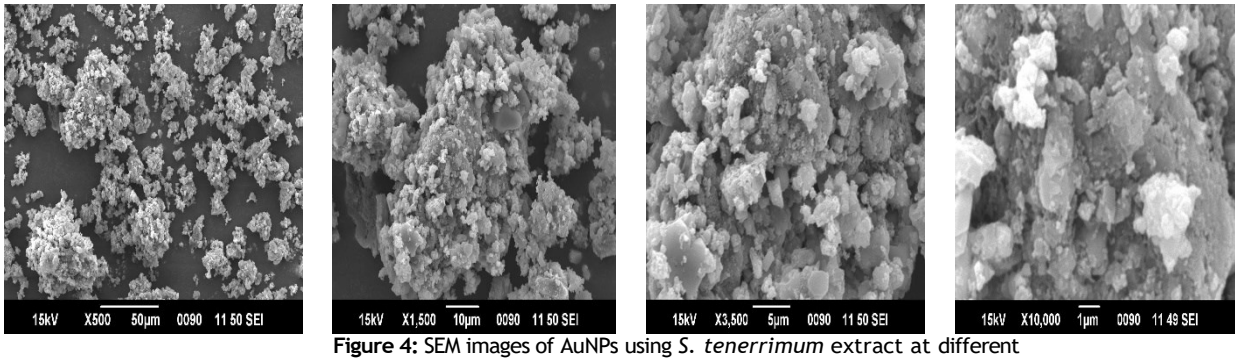

Figure 4: SEM images of AuNPs using *S. tenerrimum* extract at different magnification

3.6 X-ray energy-dispersive analysis:

The use of S. aurantium extracts in the green synthetic gold nanoparticles' basic makeup. *tenerrimum* was evaluated by the usage of edx evaluation. The gold nanoparticles created by green synthesis' edx profile the usage of *S. tenerrimum* extracts was manifested. In determining figure 5. The gold element's indications show that there are gold nanoparticles present [37]. The further signals for S, Na, O, Mg, Si, Cl, Al, Ca & K had been acquired, that originated from enzymes or proteins of *S. tenerrimum* extract. Table 2 shows the % elemental content of the gold nanoparticles that were bio-synthesized using S. *tenerrimum* extract.

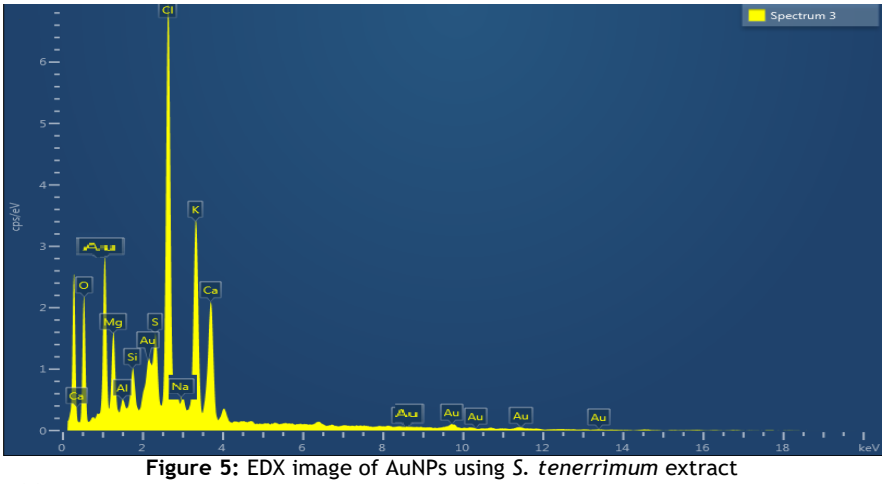

Figure 5: EDX image of AuNPs using *S. tenerrimum* extract

Table 2: Elemental composition of green synthesized AuNPs using *S. tenerrimum* extract

Element	Wt%	Atomic %
Au	70.49	31.43
O	6.76	8.87
Cl	4.72	15.8
Mg	3.03	9.23
Al	0.62	0.59
Si	1.54	1.4
S	2.95	6.35
K	3.27	8.66
Ca	3.96	5.71
Na	4.05	8.26
Total:	100	100

3.7 Transmission electron microscopy with high resolution: The green gold nanoparticles made synthetically using S. tenerrimum seaweed extracts were examined using HR-TEM to determine their size, topography, and surface morphology. As seen in Figure 6, the extracts of S. *tenerrimum* were used to create the TEM pictures of the green, synthetic gold nanoparticles. TEM images clearly show that interactions such as hydrogen bonds and electrostatic interactions between the green molecules of extracts of *S. tenerrimum* with Au^0 were a reason for the gold nanoparticle generation. TEM images (Figure 6) show that most of the green synthesized golden particles could be able to spherical with a usual dimension of about 11-20 nanometers, 9-12 nanometers & 19-26 nanometers respectively. The different growth phases of gold nanoparticles result in green synthesized gold nanoparticles [30].

The HR-TEM image (Figure 8) shows slight grid stripes on the gold nanoparticle's surface. An interplanar distance of 0.23 nm and 0.20 nm results from the stripe pattern. The fcc crystal lattice of gold nanoparticles [39]. The selected surface electric diffraction pattern (SAED) has two rings that correspond to planes (200) and (220) of the fcc crystal lattice of golden nanoparticles (Fig 7). Besides, the SAED image shows the biosynthesized gold nanoparticles are crystalline. Therefore, the HR-TEM and SAED results agree well with the XRD and SEM results. Similar outcomes are attained through *Couroupita guianensis* extract for the gold nanoparticles [40].

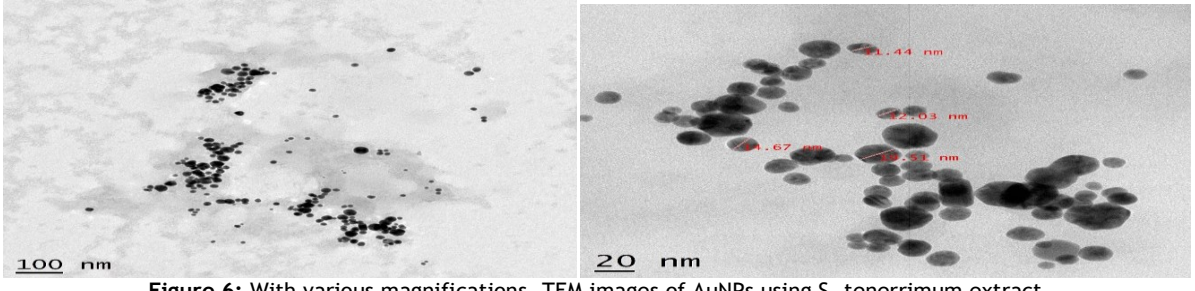

Figure 6: With various magnifications, TEM images of AuNPs using S. tenerrimum extract

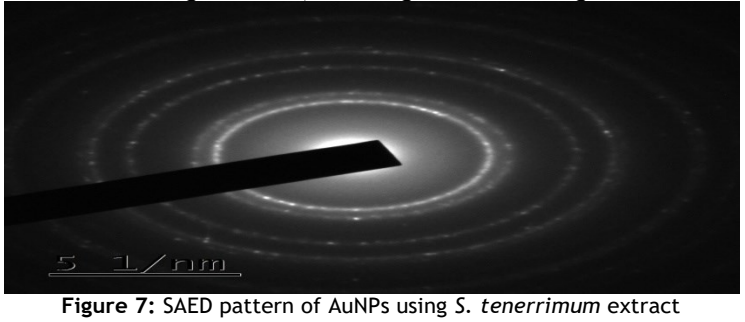

Figure 7: SAED pattern of AuNPs using *S. tenerrimum* extract

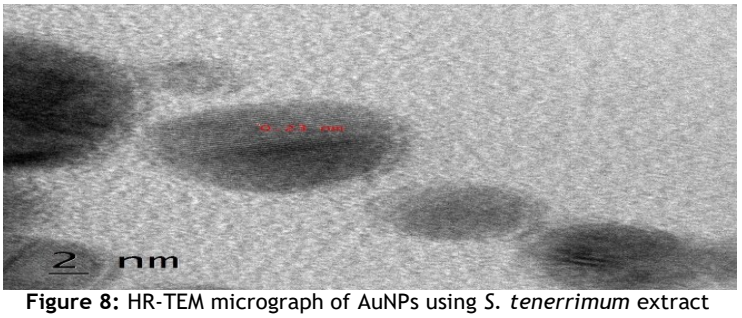

Figure 8: HR-TEM micrograph of AuNPs using *S. tenerrimum* extract

3.8 gold nanoparticles Anticancer activity:

The in vitro anticancer potential of the bio-created gold nanoparticles using S. tenerrimum seaweed extracts was evaluated using the MTT test. The cytotoxicity reviews have interpreted the usage of Table 3 for different doses (6.25, 12.5, 25, 50, 100µg/ml) of the green synthesized golden nanoparticles. Also, the golden nanoparticles of anti-cancer pursuits in opposition to the SKMEL 28 cell line are more suitable even as growing within side the dose of the gold nanoparticles. The number and timing of the green-produced gold nanoparticles affected how much capacity the SKMEL 28 cells could create. The cytotoxicity impact was moderate in the gold nanoparticles in opposition to SKMEL 28 cell lines [41, 42] shown in Fig 9 to 11.

Table 3: Anticancer activity of AuNPs using *S. tenerrimum* extract on SKMEL 28 cell line

Concentration µg/ml	% viability	IC50 µg/ml
6.25	80.76483051	52.50
12.5	69.63983051	
25	58.53601695	
50	44.60381356	
100	30.55932203	

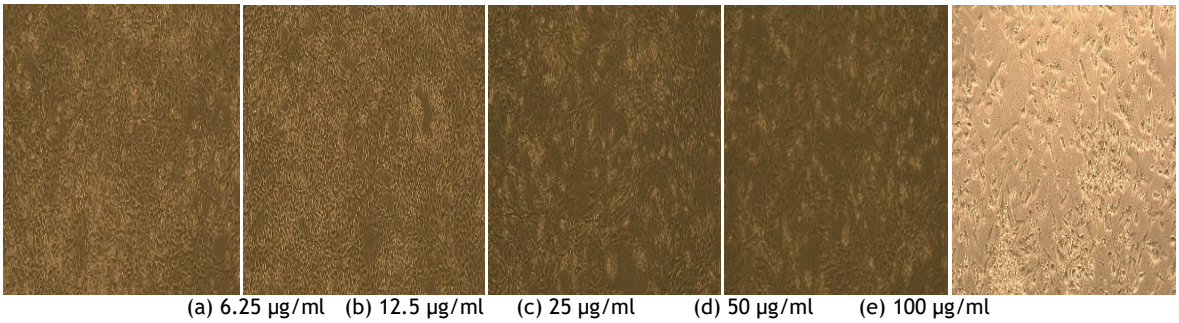

(a) 6.25 µg/ml (b) 12.5 µg/ml (c) 25 µg/ml (d) 50 µg/ml (e) 100 µg/ml

Figure 9: Effects of AuNPs through *S. tenerrimum* extract on SKMEL 28 cell line

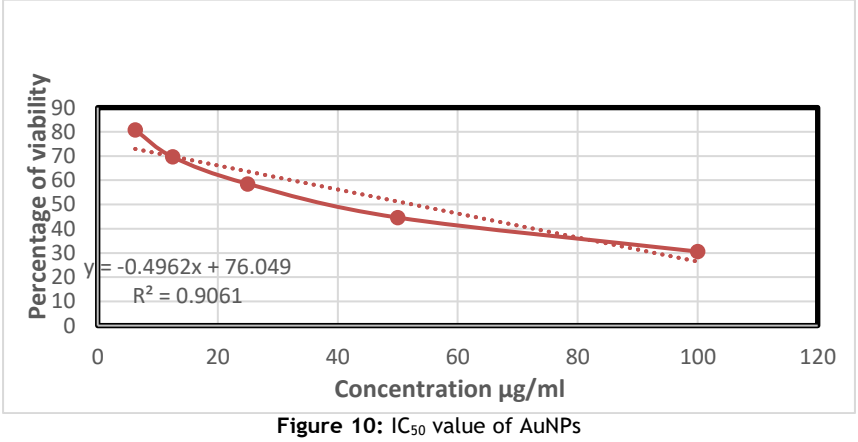

Figure 10: IC_{50} value of AuNPs

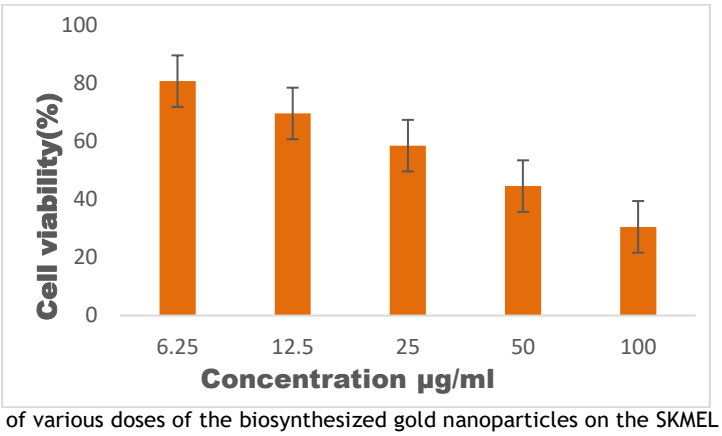

Figure 11: Cytotoxicity Effect of various doses of the biosynthesized gold nanoparticles on the SKMEL 28 cell line Catalytic activity *nitro compound reduction (p-nitroaniline & 4-nitrophenol)*

The green-activated gold nanoparticle catalytic activity is examined by selecting the nitroarenes (4-nitrophenol and b-nitroaniline) and reducing them to respective amino acids (b-phenylenediamine & 4-aminophenol). The enhancement of reaction delay is envisaged with a characteristic of the nitro compound's yellowish discoloration as well as the reactions are observed by the UV- V in spectroscopy which is represented in figure 12. The highest absorbance of a 4-nitrophenol (4-NP) aqueous solution is initiated at 317 nm and also includes the $NaBH_4$ which results in red colour absorbance from 317 to 400 nm. It is distinguished by the 4-nitropinolate ion's structure and also the colour transition from pale yellow to vivid yellow. When the nanoparticles are not presented, then the peak absorption occurred at 400nm and remained unaffected therefore the reduction process is not performed. Even though, the extra nanoparticles are synthesized from the *S. tenerrimum* aqueous extracts, after that the yellow colour solution changed into an uncoloured solution. Coherent absorption decreases with the peak maximum absorption at 400 nm presence of a recent peak at 298 nm, which is consistent with 4-aminophen (4-AP) formation which was presented in fig 12a [43]. In catalytic reduction process, the BH_4-ions based electrons are converted into nitro element through the nanoparticles and it is examined through the UV-Vis spectrophotometer. According to Figure 12a, the existence of isosceles spots converts 4-NPS to 4-NPs and has no side effects [44], and is processed in 300 seconds at ambient temperature.

In the set of Figure 12a, the absorption loop of 4-nitrophenolate at 400 nm (LnA) showed effective linear correlation and the ratio constant (K) is computed as 9.37 x 10-3s^{-1}. The reactivity of AuNPs derived from both types of alkaloids to reduce p-nitroaniline (p-NA) by including the $NaBH_4$ was studied. The NaBH4 and p-NA compound absorption spectrum represents the band at 380 nm. Even though in the AuNPs reaction compound, the band gradually reduced to 380 nanometers, however in 238 manometers, the new band forms in solution with the evolution of p-phenylenediamine (p-PDA) (Fig. 12b). While in the primary stage, p-NA molecules are absorbed on gold nanoparticles area that helps to transmit the electron. Negatively charged BH_4 electrons are transmitted to p-NA and are reduced as p-PDA increases via AuNPs & p-NA. The yellow color of p-NA is gradually disappearing because of the effective reduction of reaction in a colorless solution. The complete discoloration was observed within 140 seconds in AuNPs integrated from *S. tenerrimum*. For AuNPs combined with S tenerrimum, the value of k for the converted p-NA on p-PDA is calculated to be 16.07 x 10-3 S-1 (Figure 12 b). However, control measures are executed for the aforementioned reaction reductions by utilizing the water rather than the nanoparticle solution. The solution's golden hue was unaffected by the nitro chemicals, which confirms the nanoparticle's catalytic. For the reaction mixtures, the utilization of $NaBH_4$ concentration is comparatively higher than the nitro compounds. The reduction rate cannot depend upon $NaBH4$ concentration. Also, $NaBH_4$ concentration elevates as constant for the timely reaction. However, the outcome of the presented work exhibits the effectiveness of the catalytic than the other techniques for this condition. Biogenic AuNPs attained from *Breynia rhamnoides* are estimated to reduce 4-NP [45], the obtained k value is 7.66 x 10^{-3} S^{-1}, which is comparatively low for a reduction of 4NP. However, the attained k values for the 4-NP reduction ratio via different generations of poly(amitomine) dendrimer-metal nanocomposites (silver, platinum, palladium) indicate the catalytic ratio in the range of 0.0263 x 10^{-3} S^{-1} to 3.599 x 10^{-3} S^{-1} got to know [46]. The reduction in 4-NP was less than the results of the current research. This study's findings, there are more promising than the previous works for the further use of AuNPs. p-PDA and 4-AP are highly effective and these are the most frequently utilized intermediates in natural synthesis In medicinal products like clofibrate & paracetamol, these dyes are utilized to manufacture this product with fur dye, sulphur dye also the azo dye. Therefore, the aforementioned technique is purely natural, The creation of gold nanoparticles using a straightforward & more efficient method.

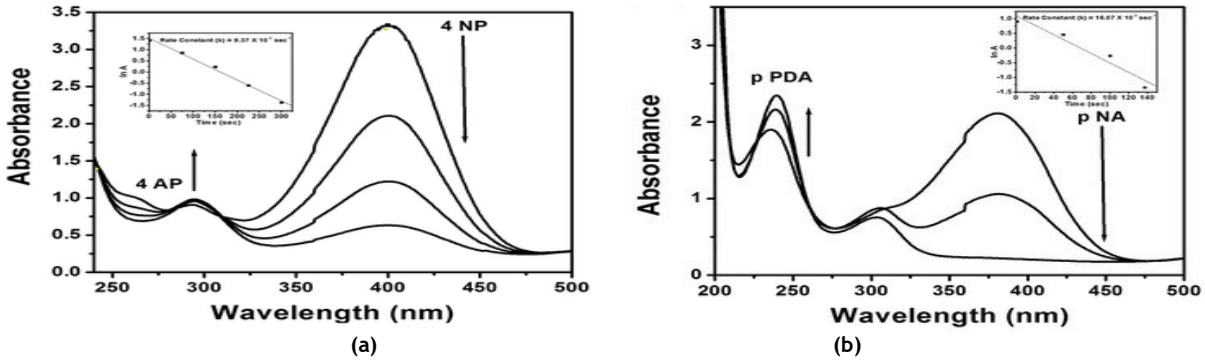

Figure 12: When 4-NP and p-NA were reduced by borohydride using AuNPs from S. tenerrimum as the catalyst, a time-dependent UV-visible spectrum was obtained (a, b).

The proper kinetic plots of ln A (A = absorbance of a 4-nitrophenolate ion at 400 nm) vs. time are shown in the inset graphics. *Organic dyes molecule reduction (Rhodamine B and Sulforhodamine 101)*

UV–Vis spectrum's Rhodamine B (Rhb) [47] has a specific feature as the peak range of absorption is occurred at 553 nm and figure 13 illustrates the discoloration of Rhb. When the sodium borohydride is not presented then the AuNPs do not reduce the dye. Once the solution of dye is integrated with the $NaBH_4$ the reduction progression begins and the dye colour becomes faded. The Rhb spectrum absorption (km max 553 nm) is decomposed for various time limits because of the existence of AuNPs derived from S. tenerimum is presented in figure 13. The reaction ranges are computed by including the logarithmic ranges of the absorbance (LnA) 553 nm based on the time as well as the layers illustrating the better correlation. The insertion diagrams in figure 13 represent the ln A and the time plots as well as constant values for reduction. To achieve the degradation execution of Sulforhodamine 101, the same implementation has been processed.

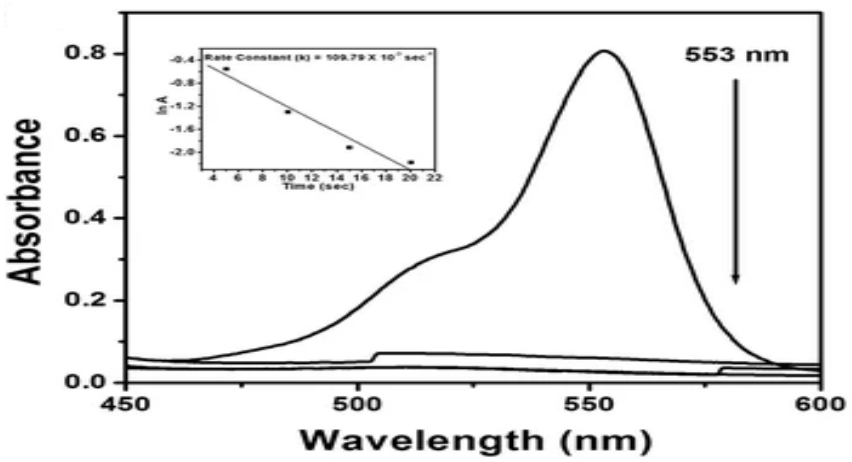

Figure 13: Using AuNPs made from S tenerrimum, Rhodamine B may be reduced catalytically at 553 nm using the UV-visible absorption spectrum. The inset plots provide the associated kinetic graphs of ln A (A = absorbance at 553 nm) vs. time.

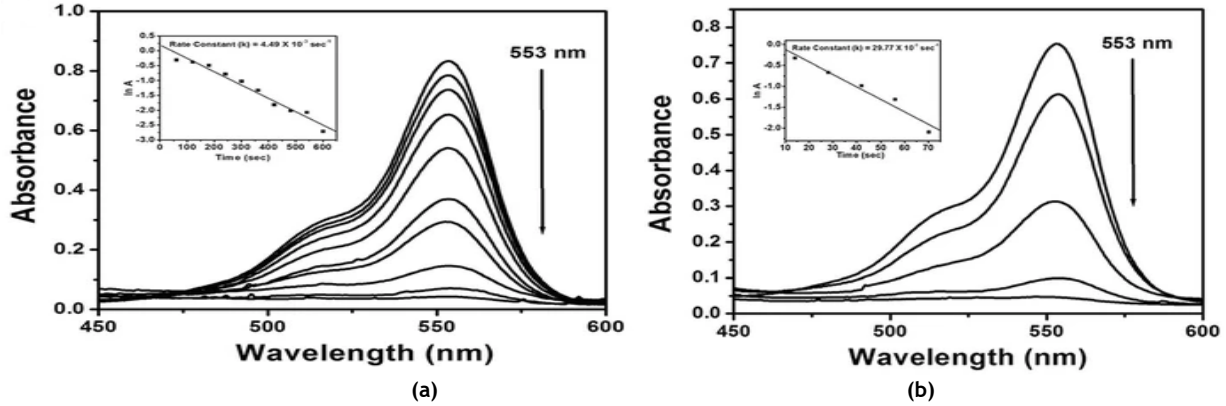

(a) **(b)**

Figure 14: The catalytic reduction of Rhodamine B at 553 nm with NaBH4 generated S tenerrimum as seen by the UV-visible absorption spectra using 10 and 25 l of AuNPs as a catalyst. The inset plots provide the ln A (A = absorbance at 553 nm) vs. time kinetic graphs that relate to it.

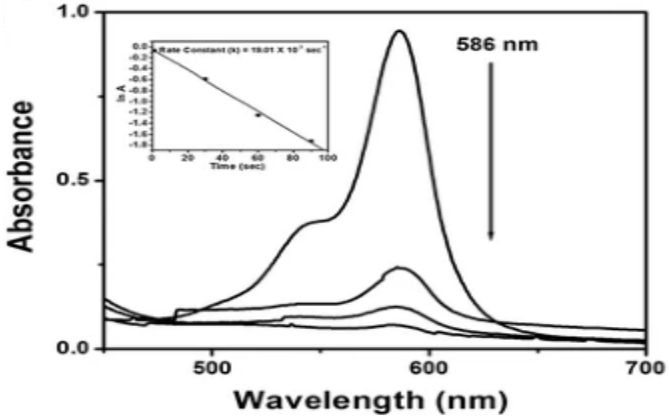

Figure 15: AuNPs derived from S tenerrimum provide the Sulforhodamine 101's catalytic reduction at 586 nm: UV-visible absorption spectrum. The inset graphs provide the corresponding kinetic plots of ln A (A = absorbance at 586 nm) vs. time.

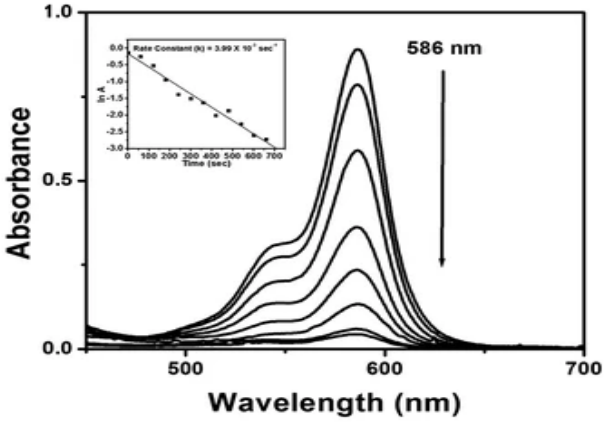

(a)

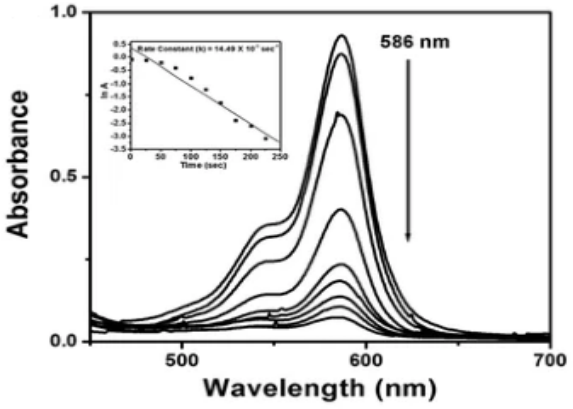

(b)

Figure 16: The spectra of UV-visible absorption for the sequential reduction of Sulforhodamine 101 at 586 nm with NaBH4 using catalysts comprised of 10 and 25 microliters of gold nanoparticles (AuNPs) produced from stenerrimum. The inset plots provide the matching ln A (A = absorbance at 553 nm) vs. time kinetic graphs.

Table 4: The amount of AuNPs used as a catalyst, the length of time it took to reduce the dye molecules, and the rate constant values were all determined in the presence of NaBH4.

Dye molecule's name	Added (µl) volume of AuNps	The rate constant (k) (s−1) (time taken for full reduction)
Rhodamine B	10	4.49×10^{-3} (600 s)
	25	29.77×10^{-3} (70 s)
	50	109.79×10^{-3} (20 s)
Sulforhodamine 101	10	3.99×10^{-3} (660 s)
	25	14.49×10^{-3} (225 s)
	50	19.01×10^{-3} (90 s)

According to the concentration of nanoparticles, the catalytic ratios of the dye reductions are accomplished. For the three catalyst fluxes, the concentration range of AuNPs is different, whereas the remaining conditions become unchanged. With increasing AuNPs concentration, k increased because of the large reaction sites (Fig. 13, 14, 15, and 16; Table 4). Table 4 illustrates the reduction time and the k value with different magnitude catalysts. Catalyst rates are added above 50 µl, 25 µl to the medium, and less than 10 µl, thus showing a dose dependence. The spectrum obtained in the image. 13, 14, 15, and 16 show that the dye molecules become completely colorless with no side products as the absorption decreases across all wavelengths. Studies conducted in the past have demonstrated that the hydroxyl, carboxyl, and amino groups functioned as efficient sources for the absorption of dye molecules[48]. The FTIR spectra result illustrates that the extract contains hydroxyl and amino groups as well as integrated gold nanoparticles. Once the dye molecules have conducted with the catalyst surface area then the electrons are transmitted effectively. The dye molecules are decreased to solve without colour as the reduction process progresses, in which the NaBH4 molecules transmit the electrons into them via golden nanoparticles.

CONCLUSION

In this study, the extract of *S. tenerrimum* aqueous is selected for the gold nanoparticles green synthesis process. The presence of green molecules was confirmed by FTIR analysis in aqueous extracts of *S. tenerrimum*, which served as a capping and reducing agent for the creation of AuNPs. The aggregated AuNPs have a crystalline property and it is spherical with dimension of 11 to 20 nm. The AuNPs provide an effective cytotoxicity effect rather than the SK MEL-28 and exhibited IC_{50} values of 52.50 µg/ml. therefore, these are inducing future research in the enhancement of biomedical drugs and integrated AuNPs serve as effective catalysts for diminishing the aromatic nitro content and natural dye molecules. The AuNPs are compiled from the *S. tenerrimum* and which gives good catalytic activity. The current green synthesis method can be expanded to produce different metal nanoparticles that may be discovered in the future for natural synthesis and extensive catalytic reactions. This is the first report from *S. tenerrimum* that deals with the anti-canceral and catalytic activity of green-integrated AuNPs.

REFERENCES

- Dubey, S.P.; Lahtinen, M.; Sä rkkä , H.; Sillanpä ä , M. Bio-prospective of *Sorbus aucuparia* leaf extract in development of silver and gold nano colloids. Colloids Surf. 2010, B 80, 26–33.
- Das,S.; Marsili, E. A green chemical approach for the synthesis of gold nanoparticles: characterization and mechanistic aspect. Rev. Environ. Sci. Biotechnol. 2010, 9, 199–204.
- Edison, T.J.I.; Sethuraman, M. Instant green synthesis of silver nanoparticles using *Terminalia chebula* fruit extract and evalua- tion of their catalytic activity on reduction of methylene blue. Process Biochem. 2012, 47, 1351–1357.
- Ghosh, S.; Patil, S.; Ahire, M.; Kitture ,R.; Gurav, D.D.; Jab-gunde, A.M.; Kale, S.; Pardesi, K.; Shinde ,V.; Bellare, J. *Gnidia glauca* flower extract mediated synthesis of gold nanoparticles and evaluation of its chemocatalytic potential. J. Nanobiotechnol. 2012,10, 17.
- Dahl, J.A.; Maddux, B.L.; Hutchison, J.E. Toward greener nanosynthesis. Chem. Rev. 2007, 107, 2228–2269.
- Doane ,T.L.; Burda, C. The unique role of nanoparticles in nanomedicine: imaging, drug delivery and therapy. Chem. Soc. 2012, Rev. 41, 2885–2911.
- Narayanan, K.B.; Sakthivel, N. Green synthesis of biogenic metal nanoparticles by terrestrial and aquatic phototrophic and heterotrophic eukaryotes and biocompatible agents. Adv. Colloid Interface Sci. 2011, 169, 59–79.
- Sadhasivam ,S.; Shanmugam, P.; Veerapandian ,M.; Subbiah, R.; Yun, K. Biogenic synthesis of multidimensional gold nanopar- ticles assisted by *Streptomyces hygroscopicus* and its electro- chemical and antibacterial properties. Biometals 2012,25, 351–360.
- Lengke, M.F.; Sanpawanitchakit ,C.; Southam ,G. Biosynthesis of gold nanoparticles: a review. In: M. Rai,

N.Duran (eds.) Metal nanoparticles in microbiology. 2011,pp. 37–74. Springer, Berlin.
- Dumur, F.; Guerlin, A.; Dumas, E.; Bertin, D.; Gigmes, D.; Mayer, C.R. Controlled spontaneous generation of gold nanoparticles assisted by dual reducing and capping agents. Gold Bull. 2011, 44, 119–137.
- Inbakandan, D.; Venkatesan, R.; Khan ,S.A. Biosynthesis of gold nanoparticles utilizing marine sponge *Acanthella elongata* (Dendy, 1905). Colloids Surf. 2010, B 81, 634–639.
- Kim, S.K. Handbook of Marine Macroalgae: Biotechnology and Applied Phycology. 2011,Wiley, Chichester.
- Chanda ,S.; Dave, R.; Kaneria, M.; Nagani, K. Seaweeds: a novel, untapped source of drugs from sea to combat infectious diseases. In: Méndez-Vilas, A. (ed.) Current Research, Technol- ogy and Education Topics in Applied Microbiology and Micro- bial Biotechnology. 2010,pp. 473–480. Formatex Research Center, Badajoz, Spain.
- Mohamed ,S.; Hashim, S.N.; Rahman ,H.A. Seaweeds: a sustainable functional food for complementary and alternative therapy. Trends Food Sci. Technol. 2012, 23, 83–96.
- Swaminathan, S.; Murugesan, S.; Damodarkumar, S.; Dhamoth- aran , R.; Bhuvaneshwari, S. Synthesis and characterization of gold nanoparticles from alga *Acanthophora spicifera* (VAHL) Boergesen. Int. J. Nanosci. Nanotechnol. 2011,2, 85–94.
- Oza ,G.; Pandey ,S.; Mewada ,A.; Kalita ,G.; Sharon, M.; Phata, J.; Ambernath ,W.; Sharon ,M. Facile biosynthesis of gold nanoparticles exploiting optimum pH and temperature of fresh water algae *Chlorella pyrenoidusa*. Adv. Appl. Sci. Res. 2012, 3, 1405–1412.
- Rajasulochana ,P.; Krishnamoorthy, P.; Dhamotharan ,R. Potential application of *Kappaphycus alvarezii* in agricultural and pharmaceutical industry. J. Chem. Pharm. Res. 2012, 4, 33–37.
- Singaravelu ,G.; Arockiamary ,J.; Kumar, V.G.; Govindaraju ,K. A novel extracellular synthesis of monodisperse gold nanoparti- cles using marine alga. *Sargassum wightii* Greville. Colloids Surf. 2007, B 57, 97–101.
- Dhas, T.S.; Kumar, V.G.; Abraham, L.S.; Karthick ,V. Govindaraju ,K. *Sargassum myriocystum* mediated biosynthesis of gold nanoparticles. Spectrochim. Acta, 2012, Part A 99, 97–101.
- Rajathi, F.A.A.; Parthiban ,C.; Kumar, V.G.; Anantharaman, P. Biosynthesis of antibacterial gold nanoparticles using brown alga. *Stoechospermum marginatum* (Kützing). Spectrochim. Acta, 2012,Part A 99, 166–173.
- Cui, W.; Li, J.; Zhang ,Y.; Rong, H.; Lu ,W.; Jiang, L. Effects of aggregation and the surface properties of gold nanoparticles on cytotoxicity and cell growth. *Nanomed. Nanotechnol. Biol. Med.*; 2012, 8:46–53. j. nano. 2011.05.005.
- Orendorff ,C.J.; Sau ,T.K.; Murphy, C.J. Shape-dependent plas- mon-resonant gold nanoparticles. Small 2, 2006, 636–639.
- Wong, Y.; Yu ,J. Laccase-catalyzed decolorization of synthetic dyes. Water Res. 1999, 33, 3512–3520.
- Banat, I.M.; Nigam, P.; Singh, D.; Marchant ,R. Microbial decolorization of textile-dye containing effluents: a review. Bioresour. Technol. 1996, 58, 217–227.
- Srinivasan, A.; Viraraghavan, T. Decolorization of dye wastewaters by biosorbents: a review. J. Environ. Manag. 2010, 91, 1915–1929.
- Mosmann ,T. et al. Immunol J. Methods 1983,65, 55–63.
- Gangula ,A.; Podila, R.; Ramakrishna, M.; Karanam ,L.; Janardhana ,C.; Rao, A.M. Catalytic reduction of 4-nitrophenol using biogenic gold and silver nanoparticles derived from *Brey- nia rhamnoides*. Langmuir 27, 2011, 15268–15274.
- Siddhardha, R.S.; Kumar ,V.L.; Kaniyoor, A.; Muthukumar, V.S.; Ramaprabhu ,S.; Podila, R.; Rao ,A.; Ramamurthy, S.S. Synthesis and characterization of gold graphene composite with dyes as model substrates for decolorization: a surfactant free laser ablation approach. Spectrochim. Acta, Part A 133, 2014, 365–371.
- Kumari ,M.; Mishra, A.; Pandey ,S.; Singh ,S.P.; Chaudhry ,V.; Mudiam ,M.K.R; Shukla ,S.; Kakkar, P.; Nautiyal, C.S. Physico-Chemical Condition Optimization during Biosynthesis lead to development of Improved and Catalytically Efficient Gold NanoParticles. Scientific Reports, 2016,vol. 6, Article ID 27575, 14 pages.
- Rajasekharreddy, P.; Rani, P.U.; Sreedhar, B. Qualitative assessment of silver and gold nanoparticle synthesis in various plants: a photobiological approach. Journal of Nanoparticle Research, vol. 12, 2010, pp. 1711–1721.
- Gopinath, K.; Venkatesh, K.S.; Ilangovan ,R.; Sankaranarayanan, K.; Arumugam, A. Green synthesis of gold nanoparticles from leaf extract of Terminalia arjuna, for the enhanced mitotic cell division and pollen germination activity. Ind. Crops Prod., 2013, 50: 737-742.
- Gopinath ,K.; Gowri ,S.; Karthika ,V.; Arumugam ,A. Green synthesis of gold nanoparticles from fruit extract of Terminalia arjuna, for the enhanced seed germination activity of Gloriosa superb. J. Nanostruct. Chem., 2014, 4: 115.
- Suganthy ,N.; Ramkumar ,V.S.; Pugazhendhi, A.; Benelli, G.; Archunan, G. Biogenic synthesis of gold nanoparticles from Terminalia arjuna bark extract: assessment of safety aspects and neuroprotective potential via antioxidant, anticholinesterase, and antiamyloidogenic effects.Environ. Sci. Pollut. Res., 2017, 25: 1-16.
- Tripathy, A.; Raichur, A.M.; Chandrasekaran, N.; Prathna ,T.C.; Mukherjee, A. Process variables in biomimetic synthesis of silver nanoparticles by aqueous extract of 172 Azadirachta indica (Neem) leaves. Journal of Nanoparticle Research, vol.12, 2010, no.1, pp. 237–246.
- Priyashree ,S.; Jha, S.;Pattanayak, S.P. A review on Cressa cretica Linn: A halophytic plant. Pharmacogn Rev, 2010, vol. 4, no. 8, pp. 161–166.
- Sunita ,P.; Jha ,S.; Pattanayak, S.P.; Mishra ,S.K. Antimicrobial Activity of a Halophytic Plant Cressa cretica L, Journal of Scientific Research. 2012, vol. 4, no.1, pp. 203– 212.
- Wang ,C.; Mathiyalagan ,R.; Kim, Y.J.; Castro-Aceituno ,V.; Singh, P.; Ahn ,S.; Wang, D.;Yang, D.C. Rapid green synthesis of silver and gold nanoparticles using Dendropanax morbifera leaf extract and their anticancer activities. International Journal of Nanomedicine, vol. 11, 2016, pp. 3691–3701.
- Song, J.Y.; Jang, H.K.; Kim, B.S. Biological synthesis of gold nanoparticles using nanoparticles using Magnolia kobus and Diopyros kaki leaf extracts. Process Biochem, vol. 44, 2009, no.10, pp. 1133–1138.
- Tokeer, A.; Wani, I.A.; Lone, I.H.; Ganguly, A.; Manzoor ,N.; Ahmad, A.; Ahmedc, J.; Al- Shihri , A.S. Antifungal activity of gold nanoparticles prepwered by solvothermal method. Materials Research Bulletin, vol. 48, 2013, pp. 12–20.
- Geetha, R.; Ashokkumar ,T.; Tamilselvan, S.; Govindaraju ,K.; Sadiq, M.; Singaravelu, G. Green synthesis of gold nanoparticles and their anticancer activity.Cancer Nanotechnology, vol. 4, 2013, pp. 91–98.
- Panwar, R.; Sharm ,A.K.; Kaloti, M.; Dutt ,D.; Pruthi ,V. Characterization and anticancer potential of ferulic acid-loaded chitosan nanoparticles against ME-180 human cervical cancer cell lines. Applied Nanoscience, vol. 6, 2016, no.6, pp. 803–813.
- Raghunandan, D.; Ravishankar, B.; Sharanbasava ,D.G.; Mahesh, B.; Harsoor, V.; Yalagatti, M.S.; Bhagawanraju, M.; Venkataraman, A. Anti-cancer studies of noble metal nanoparticles synthesized using different plant extracts. Cancer Nanotechnology, vol. 2, 2011, pp. 57–65.
- Lee, K.Y.; Hwang, J.; Lee ,Y.W.; Kim, J.; Han, S.W. One-step synthesis of gold nanoparticles using azacryptand and their applications in SERS and catalysis. J. Colloid Interface Sci. 2007, 316, 476–481.
- Chen, L.J.; Ma, H.; Chen, K.; Cha, H.R.; Lee, Y.I.; Qian, D.J.; Hao, J.; Liu, H.G. Synthesis and assembly of gold

nanoparticle- doped polymer solid foam films at the liquid/liquid interface and their catalytic properties. J. Colloid Interface Sci. 2011, 362, 81–88.

- Gangula, A.; Podila ,R.; Ramakrishna ,M.; Karanam ,L.; Janardhana ,C.; Rao, A.M. Catalytic reduction of 4-nitrophenol using biogenic gold and silver nanoparticles derived from *Brey- nia rhamnoides*. Langmuir 27, 2011, 15268–15274.
- Esumi, K.; Isono, R.; Yoshimura ,T. Preparation of PAMAM- and PPI-metal (silver, platinum, and palladium) nanocomposites and their catalytic activities for reduction of 4-nitrophenol. Langmuir 20, 2004, 237–243.
- Chen, Y.; Yin, R.H.; Wu, Q.S. Solvothermal synthesis of well- disperse ZnS nanorods with efficient photocatalytic properties.J. Nanomater. 2012, 34.
- Das, S.K.; Ghosh, P.; Ghosh, I.; Guha, A.K. Adsorption of rho- damine B on *Rhizopus oryzae*: role of functional groups and cell wall components. Colloids Surf. B 65, 2008, 30–34.